5-6-64

RESEARCH ADMINISTRATION

DECLASSIFIED
CONFIDENTIAL

NASA TECHNICAL MEMORANDUM

NASA TM X-919

X64-13882

NASA TM X-919

Declassified by authority of NASA
Classification Change Notices No. 162
Dated ** 1/15/69

MEASURED HEAT-TRANSFER AND PRESSURE DISTRIBUTIONS ON THE APOLLO FACE AT A MACH NUMBER OF 8 AND ESTIMATES FOR FLIGHT CONDITIONS

by Robert A. Jones

Langley Research Center
Langley Station, Hampton, Va.

NATIONAL AERONAUTICS AND SPACE ADMINISTRATION • WASHINGTON, D. C. • APRIL 1964

CONFIDENTIAL

CONFIDENTIAL

TECHNICAL MEMORANDUM X-919

MEASURED HEAT-TRANSFER AND PRESSURE DISTRIBUTIONS ON THE APOLLO FACE AT A MACH NUMBER OF 8 AND ESTIMATES FOR FLIGHT CONDITIONS

By Robert A. Jones

Langley Research Center
Langley Station, Hampton, Va.

[redacted]

CLASSIFIED DOCUMENT—TITLE UNCLASSIFIED

[redacted]

NATIONAL AERONAUTICS AND SPACE ADMINISTRATION

[redacted]

DECLASSIFIED

MEASURED HEAT-TRANSFER AND PRESSURE DISTRIBUTIONS ON THE APOLLO FACE AT A MACH NUMBER OF 8 AND ESTIMATES FOR FLIGHT CONDITIONS*

By Robert A. Jones

SUMMARY

Heat-transfer and pressure distributions on the front face of a model of the Apollo reentry configuration have been measured at a Mach number of 8 for angles of attack from 0° to 35° and free-stream Reynolds numbers from 0.18×10^6 to 1.44×10^6 based on face diameter. Calculations of the level and distribution of laminar heat transfer at high angles of attack are presented for both the perfect-gas tunnel conditions and for the equilibrium real-air conditions for an altitude of 180,000 feet and a velocity of 32,000 feet per second. Comparison of the calculated perfect-gas and calculated real-air heat-transfer distributions indicates that the distribution of the equilibrium real air at flight conditions was very nearly the same as the perfect-gas distribution except for a small region at the windward corner. Both of these calculated distributions were in agreement with the measured data. The calculated distributions were based on two-dimensional theory and the measured pressures. The calculated stagnation-point heat-transfer rates based on two-dimensional theory and measured pressures were in reasonable agreement with the measured data when a correction factor which accounts for the three-dimensional effects was applied. The estimated convective heating rate at the stagnation point of the full-scale vehicle at the flight condition was 296 $\frac{\text{Btu}}{\text{ft}^2\text{-sec}}$ for a wall temperature of absolute zero and 269 $\frac{\text{Btu}}{\text{ft}^2\text{-sec}}$ for a wall temperature of $4,540^{\circ}$ F.

INTRODUCTION

Since convective heat transfer will have a dominant influence on the heat-shield design of the Apollo reentry vehicle, prediction of both its distribution and level is necessary. This paper is concerned with the convective heating on the face of this vehicle.

Heat-transfer and pressure data were obtained at a Mach number of 8 for angles of attack from 0° to 35° and Reynolds numbers based on free-stream conditions and face diameter from 0.18×10^6 to 1.44×10^6. The data for high

*Title, Unclassified.

[redacted]

DECLASSIFIED

angles of attack are compared with laminar theories for predicting both the distribution and level of heat transfer, and estimates of the distribution and level are made for the full-scale vehicle at an altitude of 180,000 feet and a velocity of 32,000 feet per second. Estimates of turbulent heat-transfer rates for flight conditions are also presented.

SYMBOLS

A	correction factor, $(1 + 0.81K)^{1/2}$
C_f	skin-friction coefficient
c	specific heat of wall
D	diameter of face
H_t	total enthalpy
h	local heat-transfer coefficient, $\dfrac{\rho c \tau \dfrac{dT_w}{dt}}{T_t - T_w}$
h_o	faired measured stagnation-point heat-transfer coefficient
K	ratio of minimum to maximum velocity gradients at stagnation point
k_w	conductivity of air at wall conditions
M	Mach number
N_{Nu}	Nusselt number
N_{Pr}	Prandtl number
N_{St}	Stanton number
p	local static pressure
$p_{t,2}$	stagnation pressure behind normal shock
$\dot{q}$	heat-transfer rate
R_e	Reynolds number based on local conditions external of boundary layer
$R_{\infty,D}$	free-stream Reynolds number based on face diameter

[redacted]

r_a radius of curvature of afterbody end (fig. 1)

r_c radius of corner (fig. 1)

r_n radius of curvature of nose of model (fig. 1)

r_s radius of sting (fig. 1)

s surface distance measured from center of face

T_t total temperature

T_w wall temperature

t time

V_e local velocity external of boundary layer

V_∞ free-stream velocity

x surface distance measured from stagnation point

α angle of attack

γ entry angle

μ_w viscosity of air at wall conditions

ρ density of wall

ρ_e density of air at local conditions external of the boundary layer

ρ_w density of air at wall conditions

τ thickness of wall

ϕ angular location on face measured from windward vertical line of symmetry (fig. 2)

APPARATUS AND METHODS

The investigation was conducted in the Langley Mach 8 variable-density tunnel, which is described in reference 1. Stagnation conditions for these tests were pressures of approximately 100, 300, and 1,000 lb/sq in. absolute and temperatures from 800° F to 1,050° F depending on the pressure. The Mach number in the test area was 7.95 ± 0.05.

[redacted]

DECLASSIFIED

A sketch of the configuration investigated is shown in figure 1. The model was constructed in two sections with the plane of separation of the sections normal to the axis of symmetry at the point of maximum body diameter. The face section, which contained all instrumentation, was held in place on the afterbody section by screws. Locations of thermocouples on the face are shown in figure 2. Thermocouples of 0.010-inch-diameter iron constantan wire were spotwelded to the back surface of the thin (approximately 0.030 in.) stainless-steel wall.

The pressure model had a thick wall with tubing cut flush with the outside surface to form orifices about 0.040 inch in diameter. One vertical and two horizontal rows contained a total of 37 orifices.

Heat-transfer data were obtained by using a transient testing technique. The tunnel was brought to the desired operating conditions, and then the model was rapidly injected into the airstream by a pneumatic piston. The time required for the model to pass through the tunnel boundary layer and for steady flow to be established over the model was about 0.05 second. A high-speed analog to digital data recording system was used to record the output of each thermocouple at a rate of 40 times per second.

Heat-transfer coefficients were obtained on a card programed computer by using the method of least squares to fit a second-degree curve to the temperature-time data and then by computing the time derivative of temperature. These coefficients were computed for the interval between 0.1 and 0.6 second after injection of the model. Because of these short time intervals the model surface was nearly isothermal. The lateral heat conduction at the stagnation point for an angle of attack of 32.5° was estimated to be 0.14 percent of the aerodynamic heating rate for the highest Reynolds number. For a more complete description of the data-reduction method see reference 1. The heat-transfer coefficients, with conduction neglected, are given by the equation

$$h = \frac{\rho c \tau \frac{dT_w}{dt}}{T_t - T_w} \tag{1}$$

The recovery factor was assumed to be unity in equation (1). Estimates of h based on a laminar recovery factor of 0.85 and isentropic expansion from the stagnation-point conditions to the local measured pressure indicate that the maximum error in h due to the assumption of a recovery factor of unity was 7 percent. This error is a maximum for the position farthest from the stagnation point and becomes zero at the stagnation point.

Pressure data were obtained by photographing a butyl-phthalate manometer.

[redacted]

RESULTS AND DISCUSSION

Pressure Distributions

Schlieren photographs, oil-flow patterns on the face, pressure distributions on the face, and stagnation-point locations of this configuration have been presented in reference 2 for the same test conditions and same facility as those of the present investigation. These pressure data (ref. 2) as well as some data for an angle of attack of 32.5° are presented in figure 3. The velocity gradients along the vertical line of symmetry at the stagnation point were determined by computing the velocity from the data of figure 3 and then by reading the slope of the velocity curve. The stagnation-point locations and nondimensional stagnation-point velocity gradients so determined for each angle of attack were:

α, deg	s/r_n	$\frac{d\left(V_e/V_\infty\right)}{d\left(s/r_n\right)}$
35	0.368	2.52
32.5	.357	1.90
27.5	.319	1.54
0	0	.744

In order to obtain the actual three-dimensional stagnation-point velocity gradient at angles of attack, the pressure model was constructed with a horizontal row of orifices through the estimated stagnation point (estimated by oil flow patterns) for an angle of attack of 35°. During the pressure tests this horizontal row of orifices actually corresponded to the stagnation-point location for an angle of attack of 27.5°. The pressure distribution along the horizontal plane through the stagnation point at $\alpha = 27.5^\circ$ is presented in figure 4. The fact that the data of figure 4 are not symmetrical about the vertical line of symmetry was thought to be due to a small misalinement in yaw of the model. The nondimensional stagnation-point velocity gradient in the horizontal plane was $\frac{d\left(V_e/V_\infty\right)}{d(s/r_n)} = 0.68$.

Experimental Heat-Transfer Data and Comparison With Perfect-Gas Theory

Experimentally determined heat-transfer distributions along the vertical line of symmetry are shown in figure 5. The data for angles of attack of 35° and 32.5° are compared with theoretical laminar distributions (labeled perfect-gas theory) in figure 5(a). These theoretical distributions were obtained by the method of reference 3 by using the pressure distributions of figure 3 faired to the afterbody pressure distributions given in reference 2 and assuming that the flow was two dimensional. The agreement between the measured and theoretical distributions indicates that the flow was laminar and that the flow along the vertical plane of symmetry at high angles of attack can be considered two dimensional for purposes of calculating the heat-transfer distribution. The stagnation-point locations are indicated in figure 5 for each angle of attack. These locations were determined by fairing the pressure data of figure 3 for angles of attack for which pressure data were available (35°, 32.5°, and 27.5°) and by the oil flow patterns of reference 2 for the other angles of attack. The measured stagnation-point heat-transfer coefficients are listed for each angle of attack in figure 5 and the two-dimensional values computed by the method of reference 4 with the pressure data of figure 3 are listed for angles of attack of 35°, 32.5°, and 27.5° in figure 5(a).

A comparison of the measured and calculated (two-dimensional theory, ref. 4) stagnation-point heat-transfer coefficients, $N_{Nu}/\sqrt{R_e}$, is shown in figure 6 where

$$\frac{N_{Nu}}{\sqrt{R_e}} = \frac{h}{k_w\sqrt{\frac{\rho_w}{\mu_w}}\sqrt{\frac{dV_e}{dx}}} \tag{2}$$

Two important features are shown by this comparison; first, the measured values were higher than the calculated two-dimensional values, and second, the measured and calculated two-dimensional values became closer as the angle of attack was increased. Both features were thought to be the result of three-dimensional effects. In order to estimate the magnitude of the three-dimensional effects, a correction factor based on the form suggested by Reshotko, reference 5, and verified experimentally in reference 6, was applied to the calculated two-dimensional values. This correction factor was $A = (1 + 0.81K)^{1/2}$ where K is the ratio of minimum to maximum velocity gradient at the stagnation point,

$$K = \frac{\left(dV_e/ds\right)_{min}}{\left(dV_e/ds\right)_{max}} \tag{3}$$

For two-dimensional flow $K = 0$ and the correction factor is unity; for axisymmetric flow $K = 1$ and the correction factor is 1.345 (the ratio of axisymmetric to two-dimensional stagnation-point heating). The value of K determined by the velocity gradients along the vertical and horizontal planes through the stagnation point at an angle of attack of 27.5° was 0.44. The corresponding value of the correction factor was 1.16. Applying a correction factor of 1.16 to the value for two-dimensional theory shown in figure 6 at $\alpha = 27.5^{\circ}$ would result in a value for $N_{Nu}/\sqrt{R_e}$ of about 0.53 and thus would account for a large part of the difference between the measured and theoretical two-dimensional values. As the angle of attack is increased above 27.5°, the flow would probably become more nearly two dimensional and the value of the correction factor would decrease. This assumption is based on the consideration that for an angle of attack of 45°, the stagnation point would be located at the center portion of the corner (ref. 1) and the ratio of minimum to maximum velocity gradient could then be approximated by the ratio of corner radius r_c to face radius $D/2$. (See refs. 5 and 6.) This approximation would give a correction factor for $\alpha = 45^{\circ}$ of 1.02. Values of the correction factor for angles of attack of 32.5° and 35° were found by interpolating linearly between the values for 27.5° and 45°. The three-dimensional stagnation-point heat-transfer rate obtained by applying these correction factors to the two-dimensional theory is shown in figure 6 by the dashed line. It is believed that the agreement between the three-dimensional theory and the data and the fact that both are approaching two-dimensional theory with increasing angle of attack indicate that the flow became more nearly two dimensional at the higher angles of attack.

The heat-transfer distributions along lines which are located at various angles ϕ from the vertical line of symmetry are shown in figure 7 for an angle of attack of 35°. The variation of heat-transfer rate with s/r_n was largest along the vertical line of symmetry ($\phi = 0$), and this variation decreased with increases in ϕ to $\phi = 90^{\circ}$ where the distribution was almost invariant with s/r_n. Distributions of the type shown in figure 7 were obtained at each angle of attack. The faired distributions for the three Reynolds numbers were then cross plotted as a function of ϕ and lines of constant ratio of local to stagnation-point heating rate were determined. The results are shown in figure 8 as plots of constant h/h_o on projections of the face. The perimeter of these plots is a circle representing the juncture of the face and corner. The data of figure 8 are given in ratio to the stagnation-point values at each corresponding angle of attack. The two-dimensional nature of the flow along the vertical line of symmetry at the higher angles of attack is indicated by the rather constant heat-transfer rate in planes normal to the vertical plane of symmetry. The variation of stagnation-point location with angle of attack is shown in figure 9, and the variation of stagnation-point heat-transfer rate with angle of attack is shown in figure 10. A definite increase in stagnation-point heating rate occurred with an increase in angle of attack.

Estimate of Heat Transfer for Flight Condition

Laminar boundary layer.- Estimates of the distribution and level of heat transfer for the full-scale vehicle in flight have been made for an altitude of

180,000 feet and a velocity of 32,000 feet per second which corresponds to the maximum convective heating condition for an entry angle of 7.7° (hereinafter referred to as the real-air condition). These estimates are based on the assumption that the pressure distribution for the real-air condition would be the same as the measured pressure distributions discussed previously and that the flow would be laminar. The velocities for the real-air conditions were computed by using the measured pressure data, atmospheric conditions from reference 7, and the equilibrium properties of reference 8 based on total enthalpy and local entropy taken from reference 9. The velocity gradients were determined by reading the slope of the velocity curve. The two-dimensional stagnation-point velocity gradients so determined are compared with those of the measured values (perfect-gas conditions) in the following table:

α, deg	s/r_n	$\frac{d(V_e/V_\infty)}{d(s/r_n)}$	
		Perfect gas	Real air
35	0.368	2.52	1.60
32.5	.357	1.90	1.29
27.5	.319	1.54	.95
0	0	.744	

The velocity gradient along the horizontal plane through the stagnation point at $\alpha = 27.5^\circ$ was $\frac{d(V_e/V_\infty)}{d(s/r_n)} = 0.51$ for the real-air conditions as compared with 0.68 for the perfect-gas conditions. The value of K for the real-air condition is then 0.54 as compared with 0.44 for the perfect-gas conditions.

The theoretical laminar heat-transfer distributions for real-air condition at $\alpha = 35^\circ$ and $\alpha = 32.5^\circ$ are shown in figure 5(a). The same methods used for the perfect-gas distribution were used for these calculations except that the velocities were determined as described previously. The real-air distribution is compared with the perfect-gas distribution for $\alpha = 35^\circ$ in figure 5(a). Note that these two distributions are very nearly similar, except in the small region at the windward corner, and that both agree reasonably well with the measured data.

The stagnation-point convective heat-transfer rate for the real-air condition was estimated by using: (a) the method of reference 10, (b) the two-dimensional stagnation-point velocity gradient for $\alpha = 32.5^\circ$ listed previously, (c) a three-dimensional correction factor of 1.20, (d) a full-scale diameter of 154 inches, and (e) the assumption of a wall temperature of absolute zero. The

value of the estimate for the stagnation point at $\alpha = 32.5^{\circ}$ was 296 $\frac{\text{Btu}}{\text{ft}^2\text{-sec}}$. An estimate using the same method but assuming a wall temperature of 4,540° F gave a stagnation-point value of 269 $\frac{\text{Btu}}{\text{ft}^2\text{-sec}}$.

The primary factor affecting the applicability of these estimates, which are based on pressure distributions measured at a Mach number of approximately 8, to the real-air conditions is thought to be the large difference in Mach number and its effect on pressure distribution. The Mach number for the real-air condition is approximately 29 and, although a Mach number of 8 is sufficiently high to minimize the effects of Mach number on pressure distribution, slight effects would be present. At $M = 29$ the bow shock wave would be closer and more nearly parallel to the surface than at $M = 8$ and the pressure distribution would more closely approximate that predicted by Newtonian theory. The pressure distribution measured at Mach 8 is compared with that of Newtonian theory in figure 3(b) for $\alpha = 32.5^{\circ}$. For an infinite Mach number the stagnation point would be located at the position predicted by Newtonian concepts; however, the actual stagnation-point location for the real-air conditions would be somewhere between the Newtonian location and the location found experimentally at Mach 8. Consequently, the stagnation-point velocity gradient could be slightly higher than the value used in these estimates.

The shift in stagnation-point location for the high Mach number flow of the real-air conditions and the corresponding increase in the velocity gradient and heat-transfer rate at the stagnation point could have an effect on the downstream heat-transfer rates. For the purpose of evaluating this effect, the heat-transfer rates along the vertical line of symmetry for real-air conditions were calculated as discussed previously. These rates were compared with calculated rates which were based on the same velocity gradients with the exception of those in the immediate vicinity of the stagnation point. For this vicinity the velocity-gradient distribution was distorted to give a 50-percent change. This comparison showed that, although a change in stagnation-point velocity gradient changed the heating rate at the stagnation point, the downstream heat-transfer rates were essentially equal at an s/r_n of about 0.02 from the stagnation point. Therefore, a possible increase in heat-transfer rate due to a small shift in stagnation-point location at very high Mach numbers should be confined to a small region near the stagnation point.

Turbulent boundary layer.- The possibility of transition from laminar to turbulent flow and the resulting effect on the heat transfer for the full-scale vehicle in flight will be considered. Figure 11 shows the distribution of local Reynolds number on the Apollo vehicle for two flight conditions. These local Reynolds numbers were computed by using the measured pressure distribution and real-air properties as previously discussed. One condition corresponds to the point of peak heating for an entry angle of 7.7° (the undershoot condition for which the laminar estimates discussed previously were made); the other condition corresponds to the point of peak heating for an emergency trajectory with an entry angle of 10.0°.

The Reynolds numbers shown in figure 11 are sufficiently low so that laminar flow would be expected to exist over the entire surface of a smooth vehicle. However, the possibility exists that roughness and blowing effects resulting from ablation of the heat shield could promote boundary-layer transition. Estimates of the heat-transfer rates for a fully developed turbulent boundary layer are compared with theoretical laminar rates in figure 12. The turbulent heat-transfer rates were estimated by using: (a) a flat-plate friction law and Reynolds analogy between heat transfer and skin friction; (b) gas properties evaluated at local external conditions; (c) the assumption that the boundary layer was fully turbulent from the stagnation point; and (d) the measured pressure distribution and real-air properties as previously discussed. This approach is justified as follows: (a) the effect of the pressure gradient on the velocity and temperature profiles is small and, thus, the flat-plate friction law and Reynolds analogy between heat transfer and skin friction should be valid (ref. 11); (b) at the present state of the art there seems to be no preference between local external properties or reference enthalpy properties; however, some experimental data have shown that better agreement was obtained when local external properties were used (refs. 11 and 12); and (c) the consideration that, with no knowledge of any transition condition to use, use of stagnation initial conditions can lead to reasonably accurate predictions of the turbulent heating rates at a moderate distance downstream of the transition region (ref. 13). The equations used are:

$$\frac{C_f}{2} = 0.0296R_e^{-0.2} \tag{4}$$

$$N_{St} = \frac{C_f}{2}\left(N_{Pr}\right)^{-2/3} \tag{5}$$

$$\dot{q} = \rho_e V_e H_t \frac{C_f}{2}\left(N_{Pr}\right)^{-2/3} \tag{6}$$

where the Prandtl number N_{Pr} was taken to be 0.70. The values obtained from the method outlined above are, at best, only a rough estimate of the heating rates that would exist for a fully developed turbulent boundary layer. In figure 12 only those values of turbulent heat-transfer rates are shown which are larger than the theoretical laminar values. The laminar heat-transfer rates were obtained by multiplying the theoretical distribution of figure 5(a) for an angle of attack of 32.5° by the calculated stagnation-point heating rates. Turbulent heat-transfer rates become larger than laminar rates (fig. 12) at s/r_n locations which correspond to a Reynolds number of approximately 40,000 (figs. 11 and 12). If the boundary-layer flow were to become turbulent, figure 12 indicates that the heat-transfer rate would be increased by a large amount. However, the transition criteria that would actually apply are not known, and these estimates indicate only that the possibility of boundary-layer transition should be examined.

CONCLUSIONS

Heat-transfer and pressure distributions on the front face of a model of the Apollo reentry configuration obtained at a Mach number of 8 are presented. Comparisons are made with calculated heat-transfer distributions both for a perfect gas and for an equilibrium real air at conditions for an altitude of 180,000 feet and a velocity of 32,000 feet per second. The following conclusions are made:

1. The experimental heat-transfer distributions are in agreement with calculated distributions based on two-dimensional theory and measured pressure. The calculated distributions for a perfect gas and for an equilibrium real air at flight conditions are very nearly similar except for a small region near the windward corner.

2. The calculated stagnation-point heat-transfer rates based on two-dimensional theory and measured pressures are in reasonable agreement with the measured values when a correction factor which accounts for the three-dimensional effects is applied.

Langley Research Center,
National Aeronautics and Space Administration,
Langley Station, Hampton, Va., December 12, 1963.

[redacted]

REFERENCES

1. Jones, Robert A.: Heat-Transfer and Pressure Distributions on a Flat-Face Rounded-Corner Body of Revolution With and Without a Flap at a Mach Number of 8. NASA TM X-703, 1962.

2. Jones, Robert A.: Experimental Investigation of the Overall Pressure Distribution, Flow Field, and Afterbody Heat-Transfer Distribution of an Apollo Reentry Configuration at a Mach Number of 8. NASA TM X-813, 1963. (Supersedes NASA TM X-699.)

3. Beckwith, Ivan E., and Cohen, Nathaniel B.: Application of Similar Solutions to Calculation of Laminar Heat Transfer on Bodies With Yaw and Large Pressure Gradient in High-Speed Flow. NASA TN D-625, 1961.

4. Fay, J. A., and Riddell, F. R.: Theory of Stagnation Point Heat Transfer in Dissociated Air. Jour. Aero. Sci., vol. 25, no. 2, Feb. 1958, pp. 73-85, 121.

5. Reshotko, Eli: Heat Transfer to a General Three-Dimensional Stagnation Point. Jet Propulsion, vol. 28, no. 1, Jan. 1958, pp. 58-60.

6. Gunn, Charles R.: Heat-Transfer Measurements on the Apexes of Two 60° Sweptback Delta Wings (Panel Semiapex Angle of 30°) Having 0° and 45° Dihedral at a Mach Number of 4.95. NASA TN D-550, 1961.

7. Minzner, R. A., Champion, K. S. W., and Pond, H. L.: The ARDC Model Atmosphere, 1959. Air Force Surveys in Geophysics No. 115 (AFCRC-TR-59-267), Air Force Cambridge Res. Center, Aug. 1959.

8. Korobkin, I., and Hastings, S. M.: Mollier Chart for Air in Dissociated Equilibrium at Temperatures of 2000°K to 15,000°K. NAVORD Rep. 4446, U.S. Naval Ord. Lab. (White Oak, Md.), May 23, 1957.

9. Huber, Paul W.: Hypersonic Shock-Heated Flow Parameters for Velocities to 46,000 Feet Per Second and Altitudes to 323,000 Feet. NASA TR R-163, 1963.

10. Cohen, Nathaniel B.: Boundary-Layer Similar Solutions and Correlation Equations for Laminar Heat-Transfer Distribution in Equilibrium Air at Velocities up to 41,000 Feet Per Second. NASA TR R-118, 1961.

11. Rose, Peter H., Probstein, Ronald F., and Adams, Mac C.: Turbulent Heat Transfer Through a Highly Cooled Partially Dissociated Boundary Layer. Res. Rep. 14, AVCO Res. Lab., Jan. 1958.

12. Jones, Jim J.: Shock-Tube Heat-Transfer Measurements on Inner Surface of a Cylinder (Simulating a Flat Plate) for Stagnation-Temperature Range 4,100° to 8,300° R. NASA TN D-54, 1959.

[redacted]

13. Cohen, Nathaniel B.: A Method for Computing Turbulent Heat Transfer in the Presence of a Streamwise Pressure Gradient for Bodies in High-Speed Flow. NASA MEMO 1-2-59L, 1959.

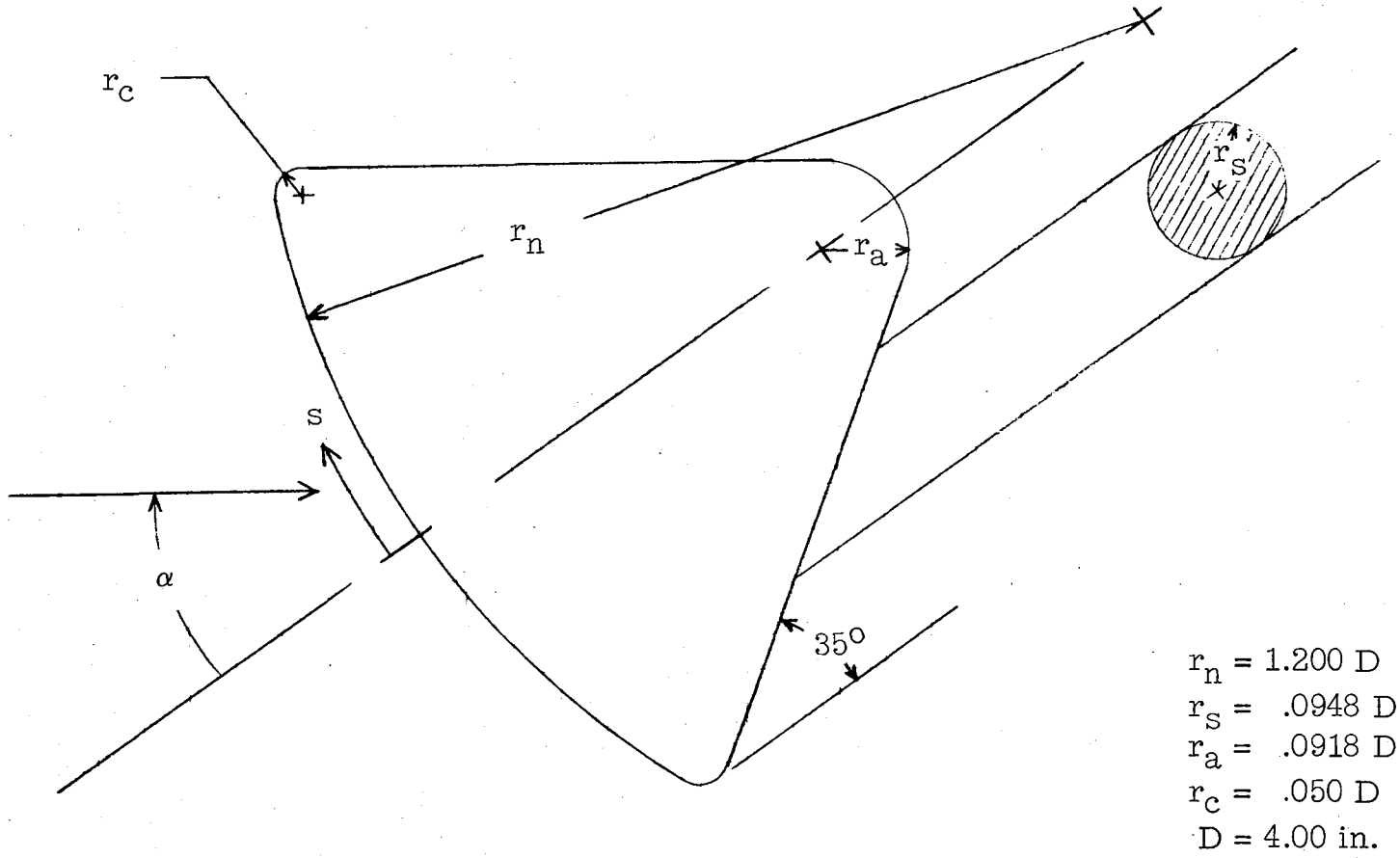

Figure 1.- Sketch of model.

CONFIDENTIAL

CONFIDENTIAL

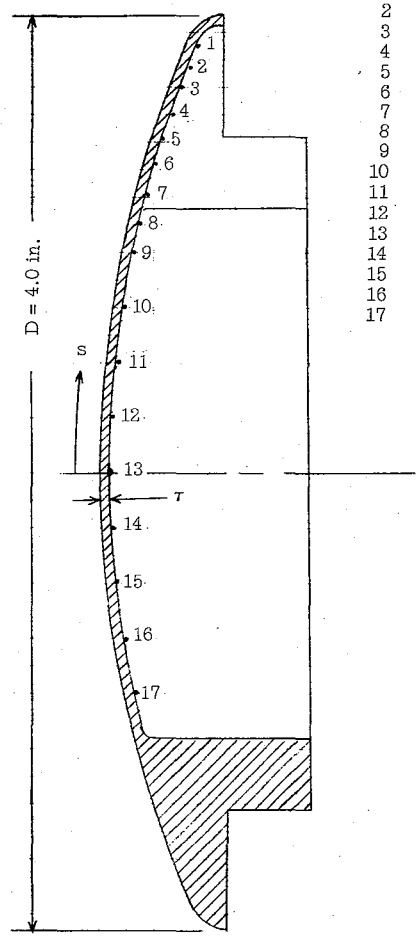

Thermocouple	s/r_n	$\dot{\tau}$, in.
1	0.402	0.0340
2	.380	.0340
3	.357	.0343
4	.331	.0345
5	.305	.0345
6	.278	.0343
7	.252	.0323
8	.227	.0318
9	.200	.0315
10	.154	.0305
11	.101	.0303
12	.502	.0300
13	0	.0295
14	-.502	.0295
15	-.101	.0295
16	-.154	.0298
17	-.200	.0305

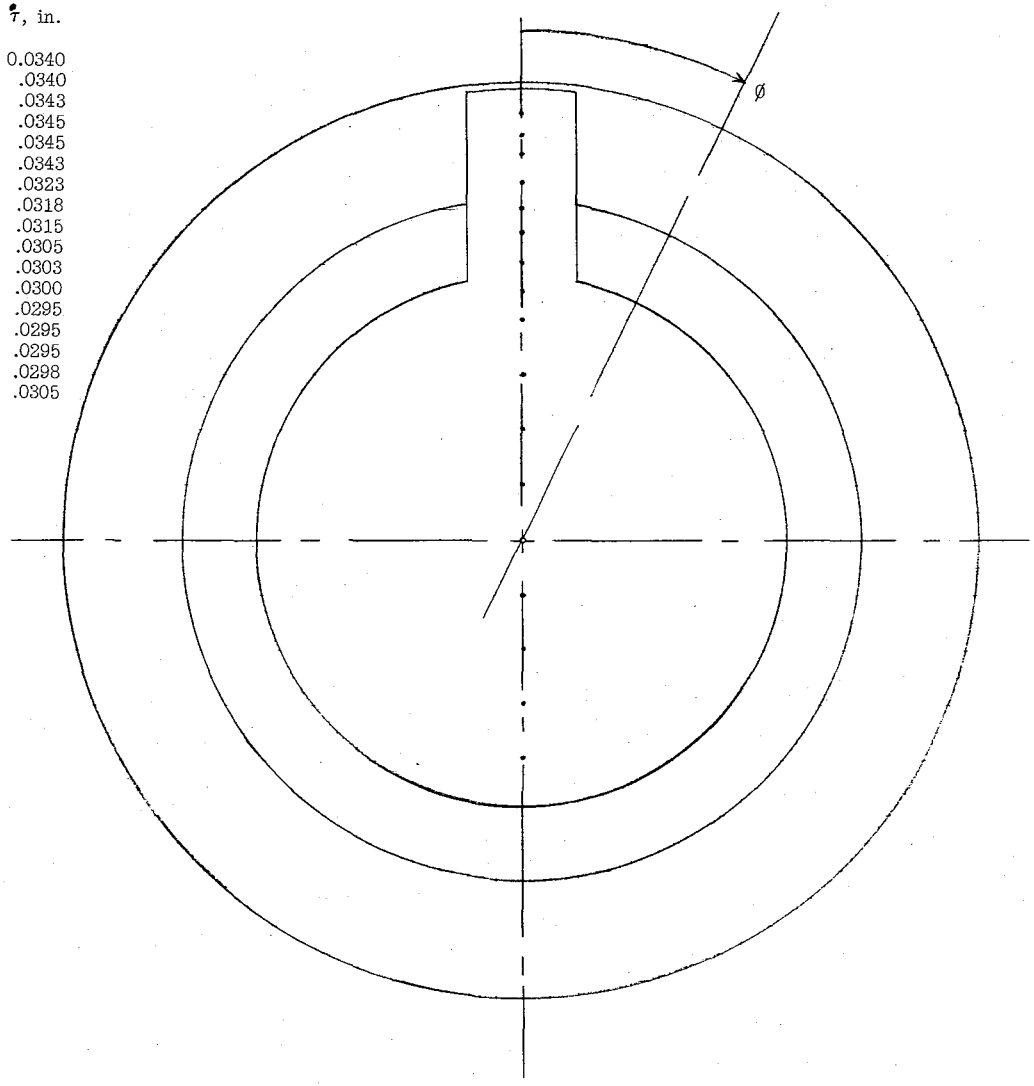

Figure 2.- Thermocouple installation.

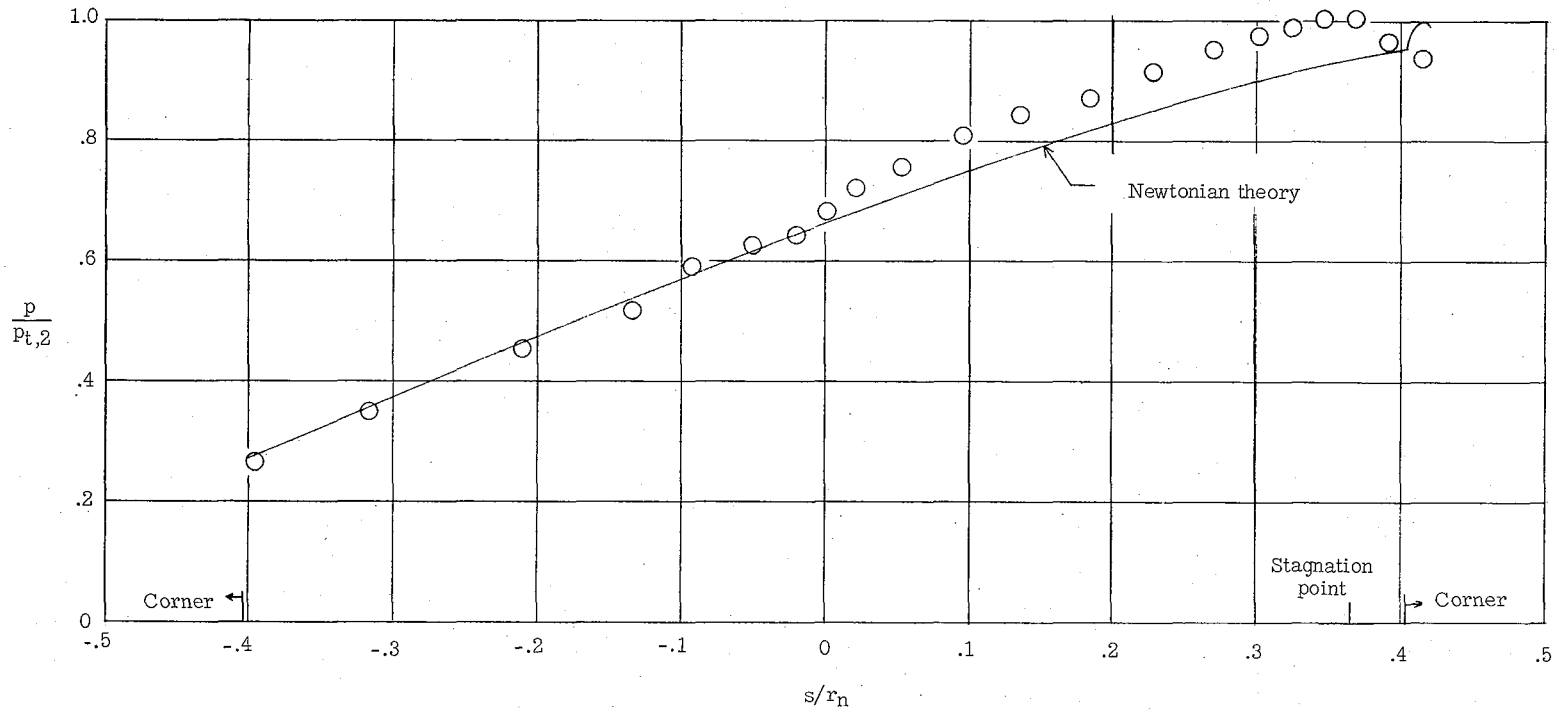

(a) $\alpha = 35^{\circ}$.

Figure 3.- Pressure distribution along vertical line of symmetry.

CONFIDENTIAL

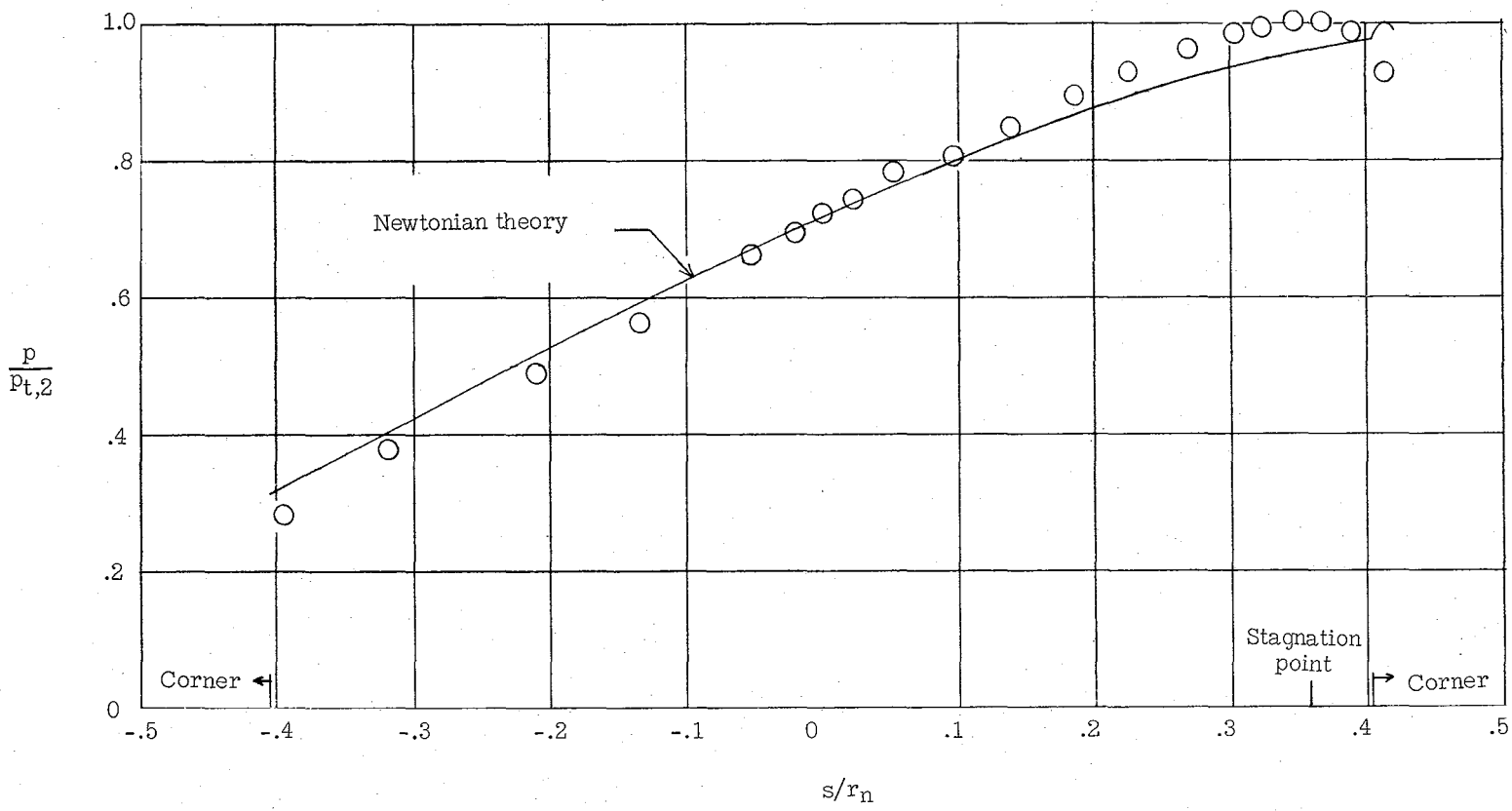

(b) $\alpha = 32.5^{\circ}$.

Figure 3.- Continued.

CONFIDENTIAL

[redacted]

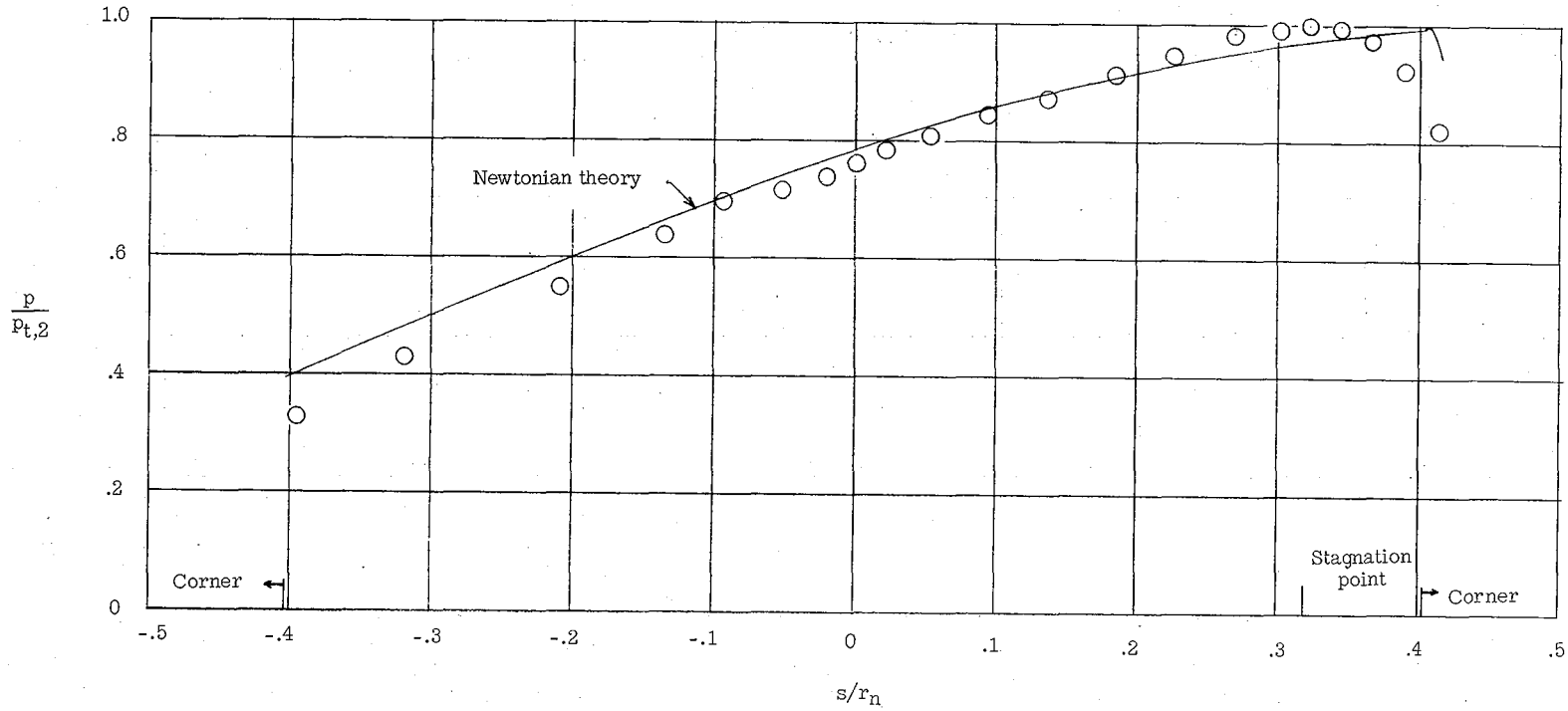

(c) $\alpha = 27.5^{\circ}$.

Figure 3.- Continued.

CONFIDENTIAL

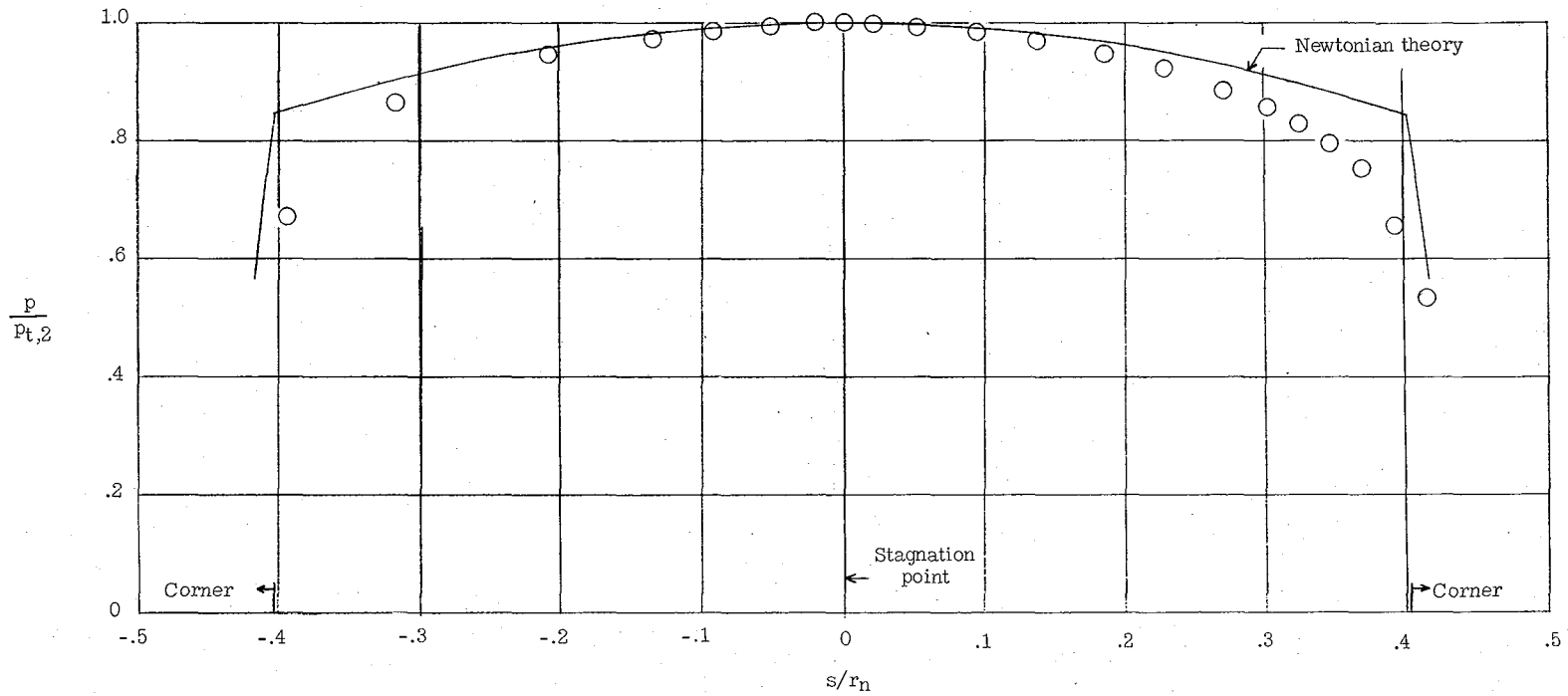

(d) $\alpha = 0^{\circ}$.

Figure 3.- Concluded.

CONFIDENTIAL

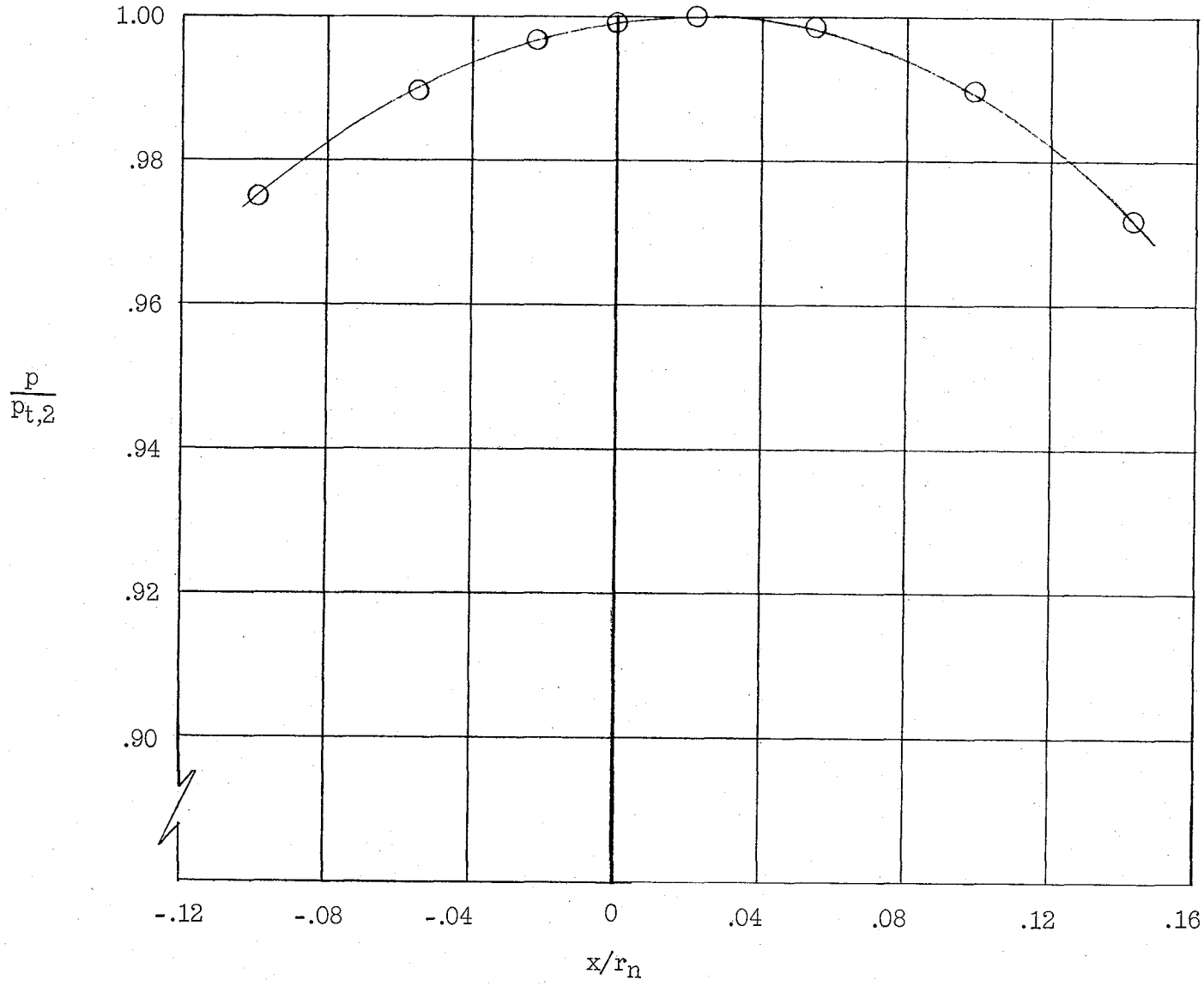

Figure 4.- Pressure distribution along horizontal plane through stagnation point at $\alpha = 27.5^{\circ}$ and $s/r_n = 0.319$.

CONFIDENTIAL

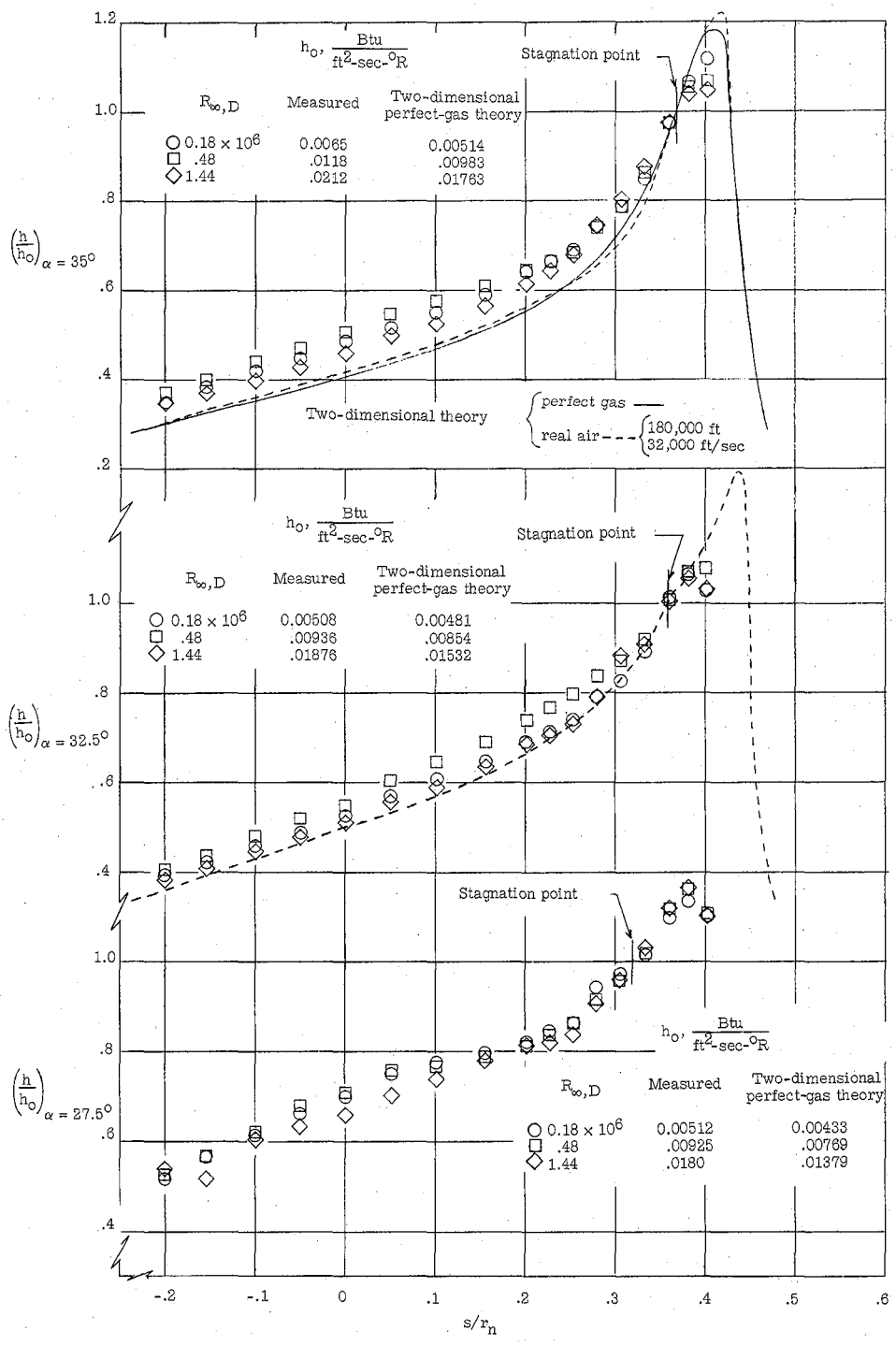

(a) $\alpha = 35^o$, 32.5^o, and 27.5^o.

Figure 5.- Heat-transfer distribution along vertical plane of symmetry.

[redacted]

DECLASSIFIED

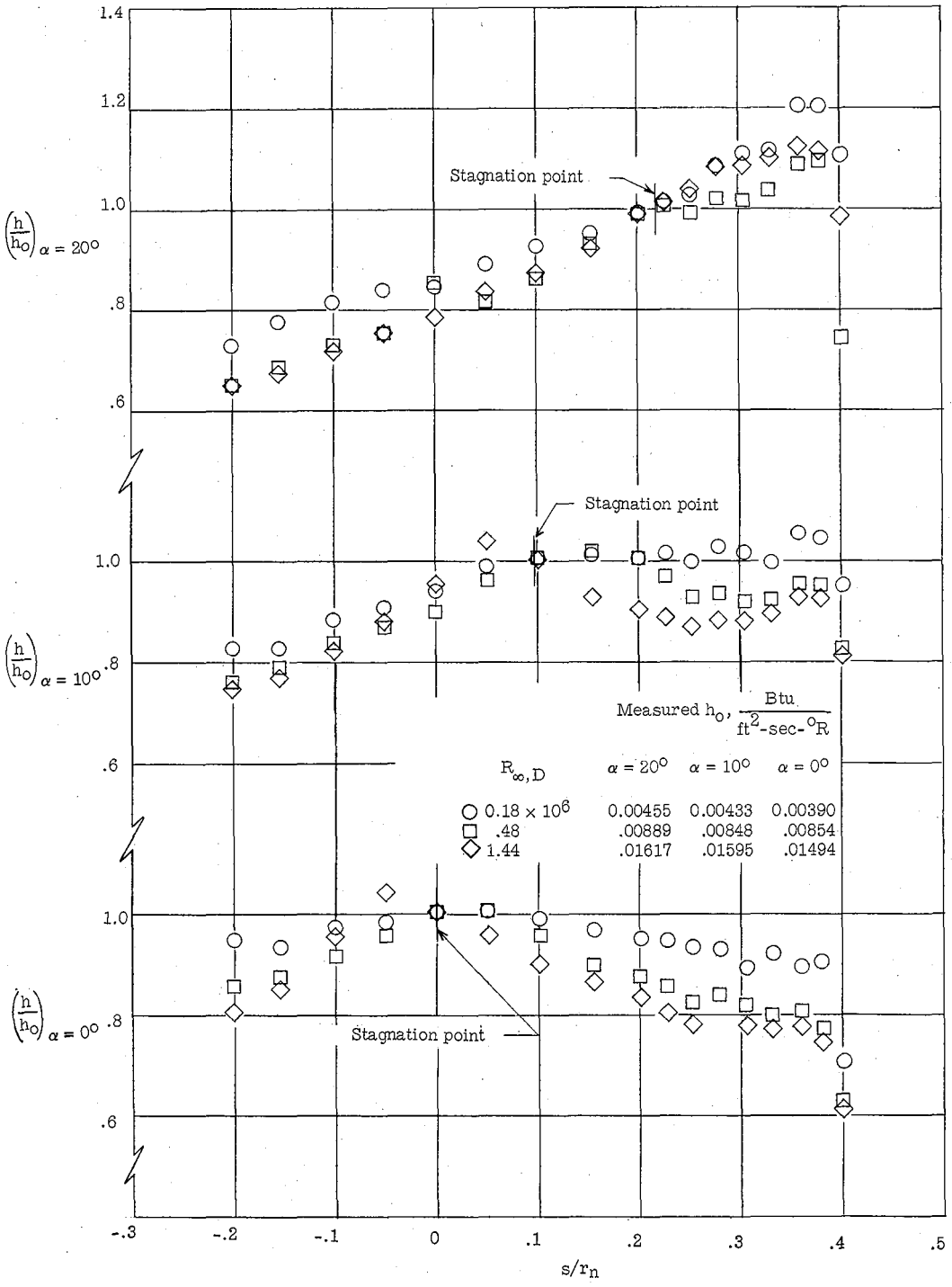

(b) $\alpha = 20^o$, 10°, and 0°.

Figure 5.- Concluded.

[redacted]

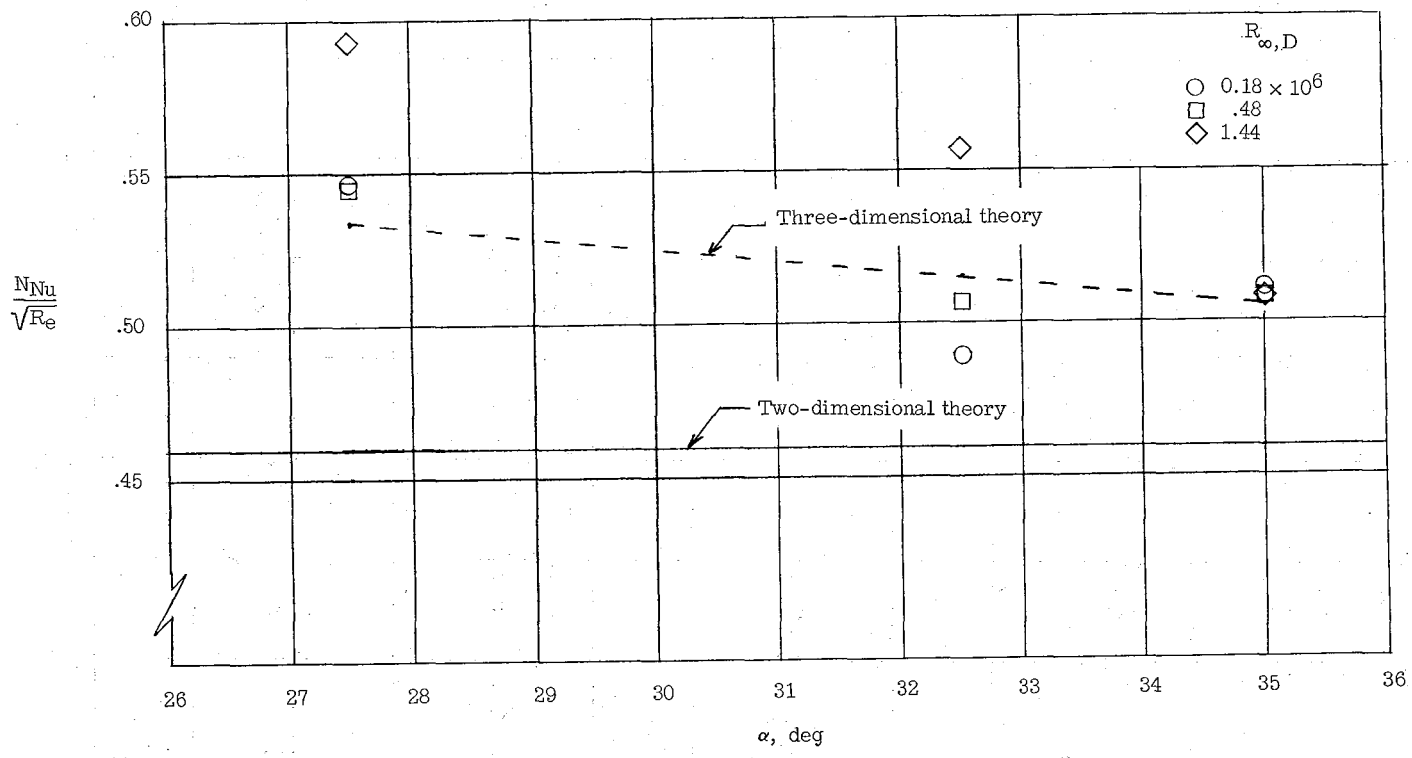

Figure 6.- Comparison of measured and calculated stagnation-point heat-transfer coefficients.

CONFIDENTIAL

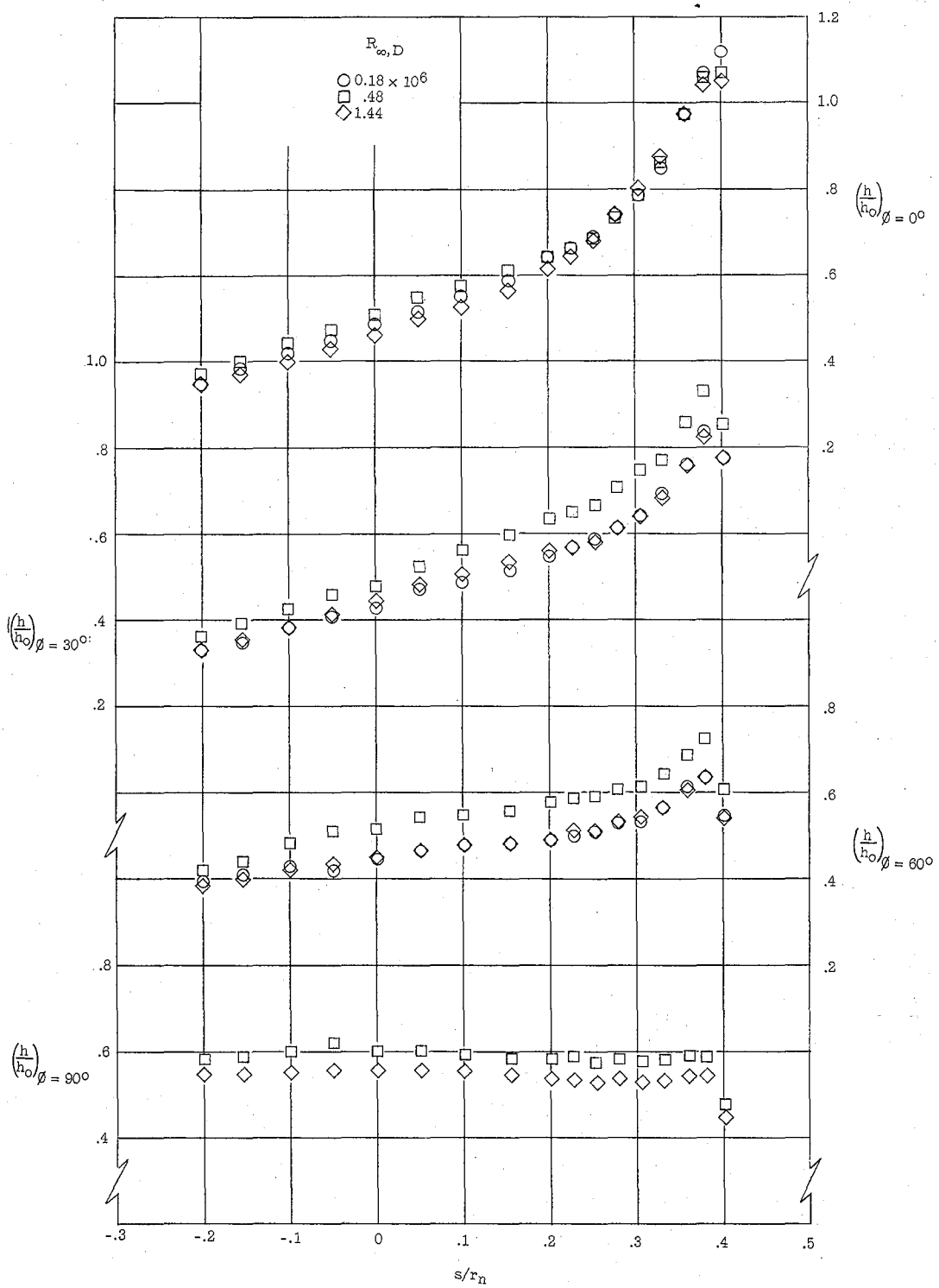

Figure 7.- Heat-transfer distribution for various values of ϕ at $\alpha = 35^\circ$.

[redacted]

CONFIDENTIAL
DECLASSIFIED

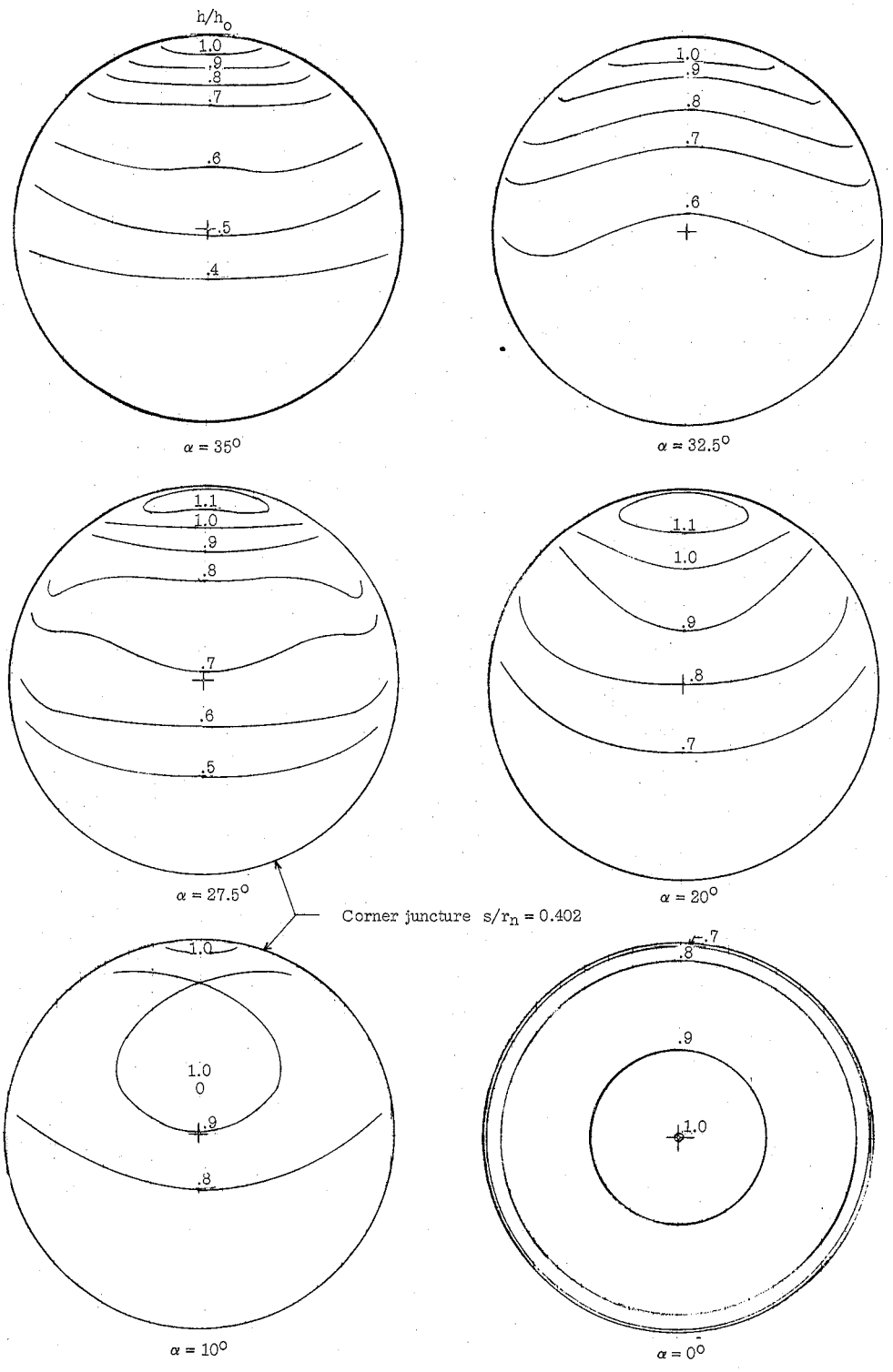

Figure 8.- Plots of constant ratio of local to stagnation-point heating rates.

[redacted]

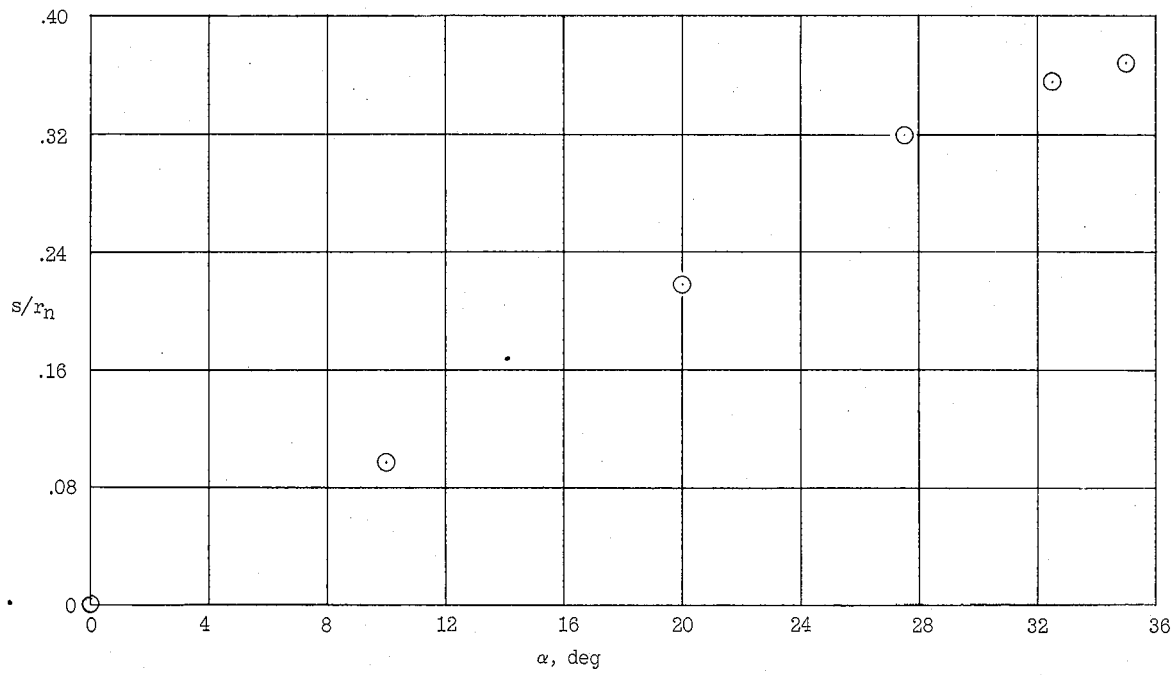

Figure 9.- Variation of stagnation-point location with angle of attack.

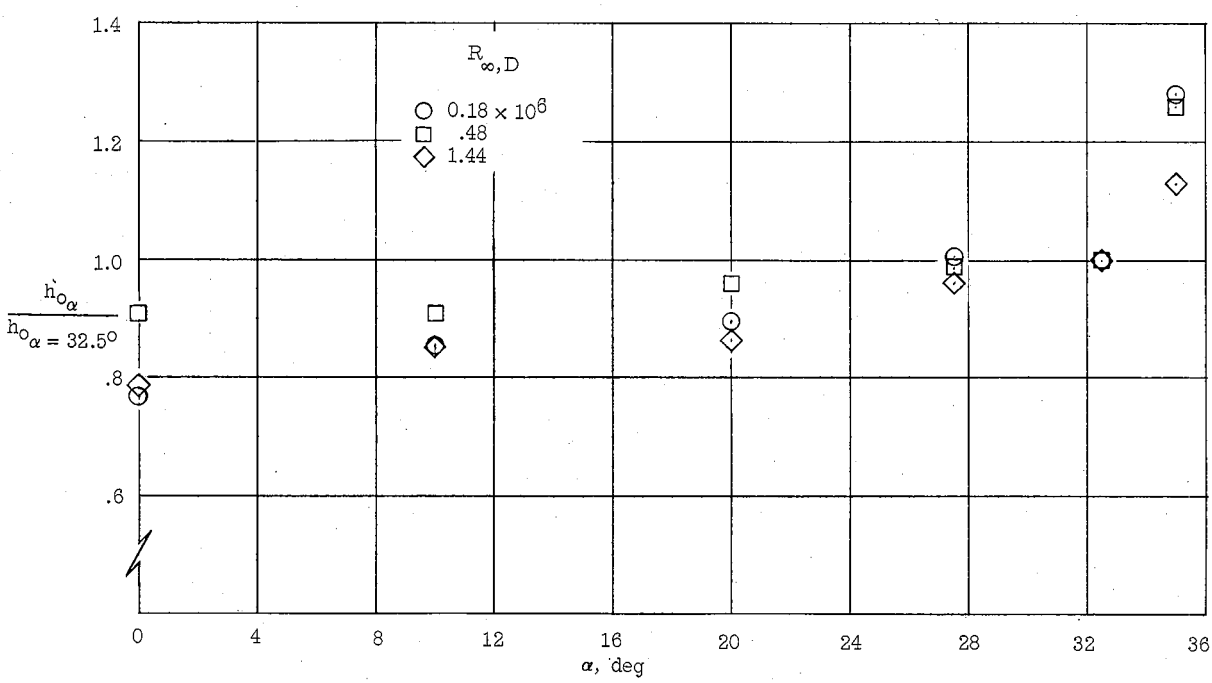

Figure 10.- Variation of stagnation-point heating with angle of attack.

[redacted]

DECLASSIFIED

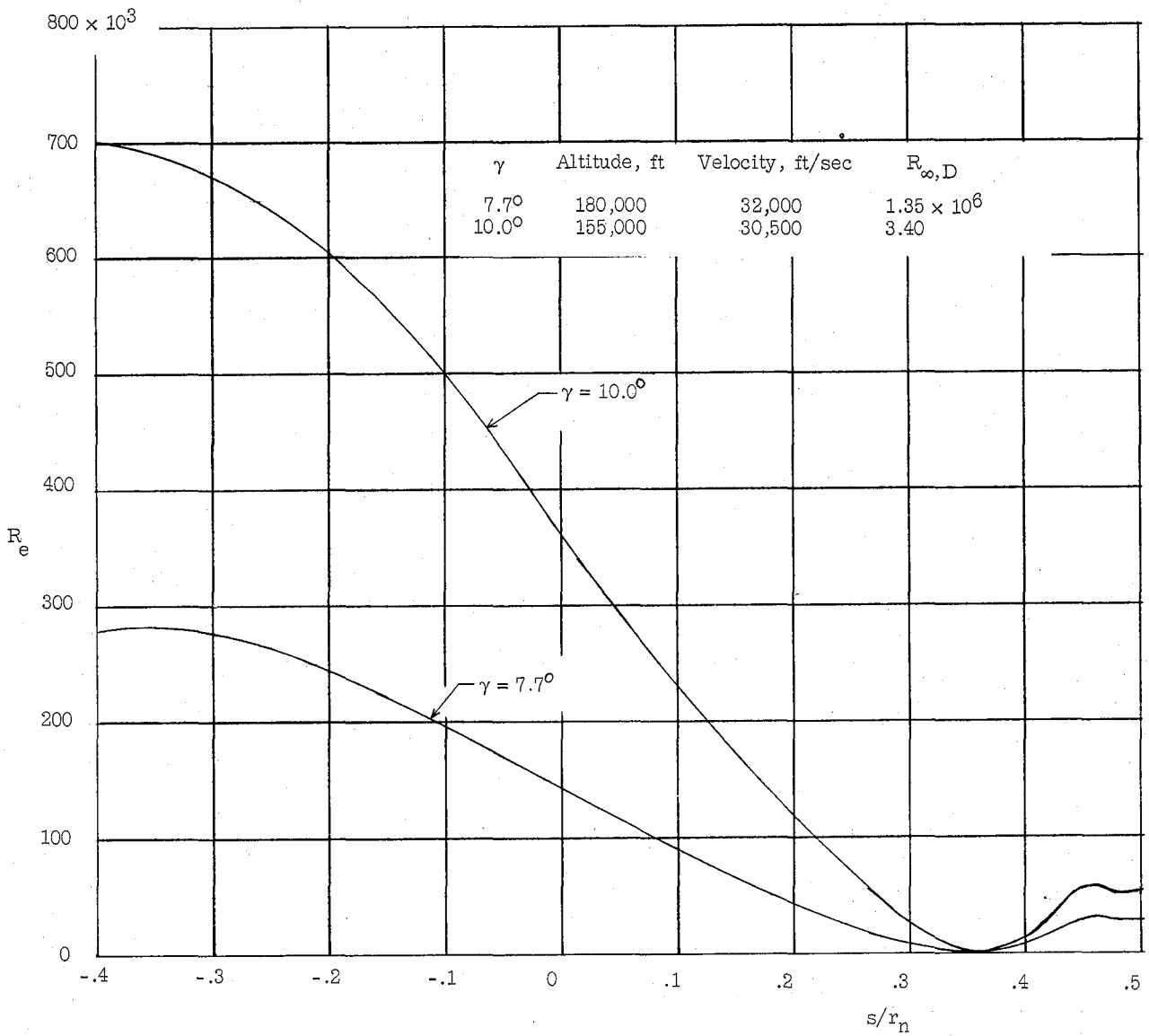

Figure 11.- Distribution of local Reynolds number along vertical plane of symmetry for an angle of attack of approximately 33°.

[redacted]

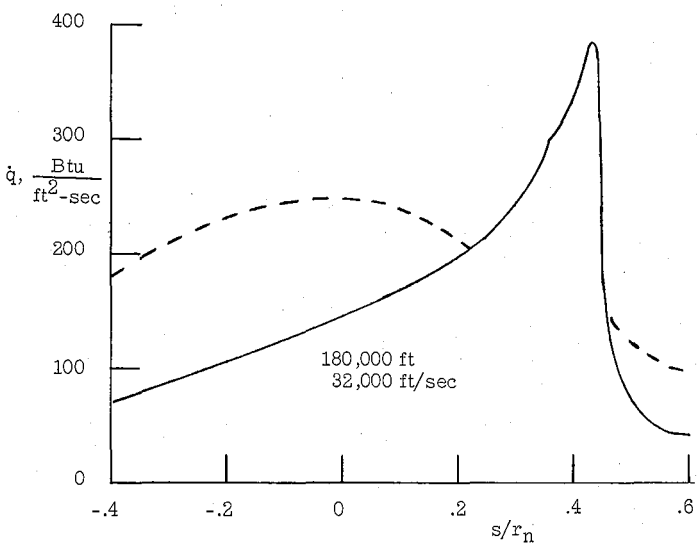

(a) $\gamma = 7.7^{\circ}$.

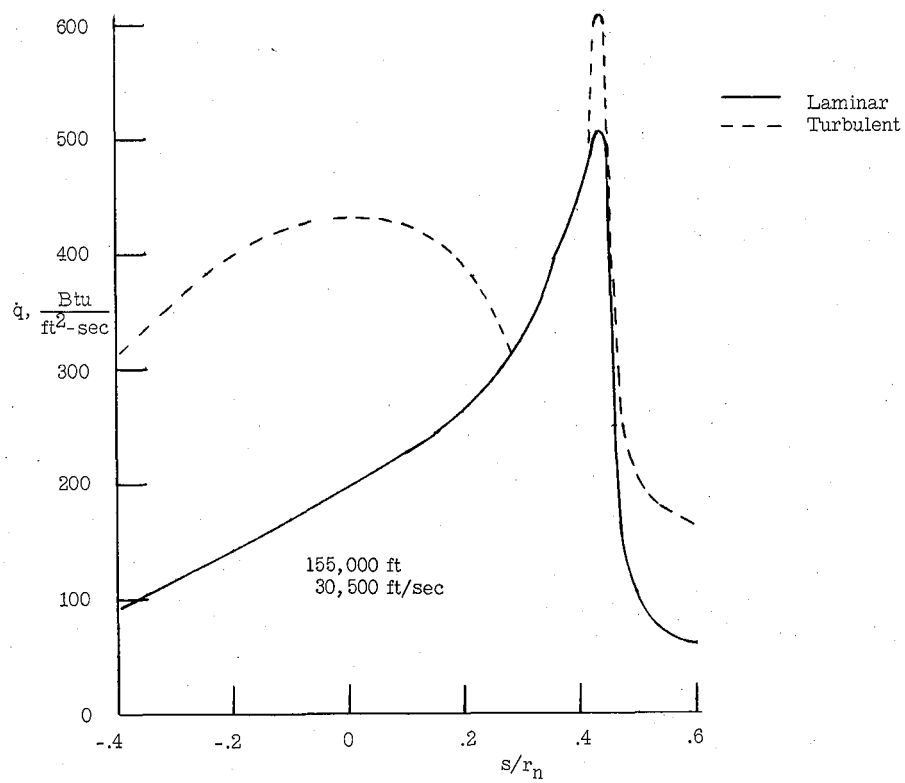

(b) $\gamma = 10.0^{\circ}$.

Figure 12.- Estimated turbulent heat-transfer rates compared with laminar values.

[redacted]

NASA-Langley, 1964 L-3554